

Controlling Latent Diffusion Using Latent CLIP

Jason Becker*
EPFL, KIT

jason.becker@epfl.ch

Chris Wendler*
Northeastern University

ch.wendler@northeastern.edu

Peter Baylies
Leonardo AI

Robert West
EPFL

Christian Wressnegger
KASTEL Security Research Labs
Karlsruhe Institute of Technology (KIT)

Abstract

Instead of performing text-conditioned denoising in the image domain, latent diffusion models (LDMs) operate in latent space of a variational autoencoder (VAE), enabling more efficient processing at reduced computational costs. However, while the diffusion process has moved to the latent space, the contrastive language-image pre-training (CLIP) models, as used in many image processing tasks, still operate in pixel space. Doing so requires costly VAE-decoding of latent images before they can be processed. In this paper, we introduce Latent-CLIP, a CLIP model that operates directly in the latent space. We train Latent-CLIP on 2.7B pairs of latent images and descriptive texts, and show that it matches zero-shot classification performance of similarly sized CLIP models on both the ImageNet benchmark and a LDM-generated version of it, demonstrating its effectiveness in assessing both real and generated content. Furthermore, we construct Latent-CLIP rewards for reward-based noise optimization (ReNO) and show that they match the performance of their CLIP counterparts on GenEval and T2I-CompBench while cutting the cost of the total pipeline by 21%. Finally, we use Latent-CLIP to guide generation away from harmful content, achieving strong performance on the inappropriate image prompts (I2P) benchmark and a custom evaluation, without ever requiring the costly step of decoding intermediate images.¹

1. Introduction

Many modern generative text-to-image models are based on latent diffusion models (LDMs) [2, 13, 28, 33]. LDMs leverage a clever computational trick to unlock the stable training

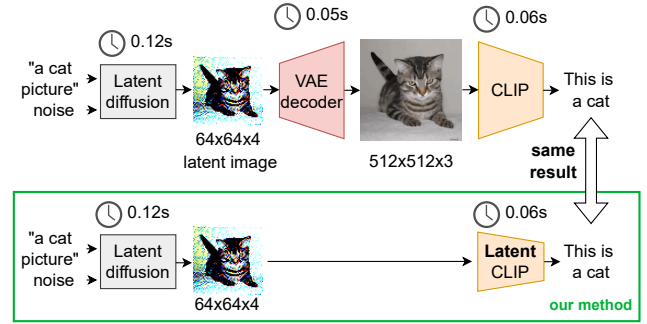


Figure 1. We propose to compute CLIP embeddings for latent images directly using Latent-CLIP (bottom) instead of VAE-decoding them first (top). Latent-CLIP can serve as a drop-in replacement of CLIP, preserving performance while saving computation. We use the technique from <https://huggingface.co/blog/TimothyAlexisVass/explaining-the-sdxl-latent-space> to compute the preview of the latent image.

dynamics of diffusion models [10] for high-resolution image synthesis: LDMs perform the text-conditioned denoising process in latent space rather than in the image domain, leveraging the lower dimensionality and reducing the computation effort decisively.

The training of LDMs is performed in two stages: In the first stage, one learns a map from high-resolution images into a much smaller space of “latent images” (and back). As an example, SDXL [36] reduces both the image width and height by a factor of 8 and increases the channel dimension by one, mapping $1024 \times 1024 \times 3$ images to $128 \times 128 \times 4$ latent images, using a variational autoencoder (VAE) [21]. In the second stage, a text-conditioned diffusion model is trained to map from input noise and a textual caption to a corresponding latent image.

This decoupling of the challenging task of creating latent images matching their textual descriptions and the task of creating high-resolution images has proven very effective,

*Equal contribution

¹We provide implementations of our Latent-CLIP powered zero-shot classification and ReNO image generation here: <https://github.com/jsonBackup/Latent-CLIP-Demo>.

and has dethroned previous generative adversarial neural network (GAN) based approaches [10]. However, while the diffusion process moved from the pixel space to the latent space, most other components of modern image processing pipelines such as image classifiers [23], image reward functions [43], image-text alignment models like CLIP [29], and visual language models [46] still operate in the image/pixel space. *As a result, latent images have to be decoded back to pixel space before any task-specific models can be used, resulting in a significant computational overhead.* Often the VAE-decoding step is even more expensive than the forward pass of the task-specific model.

In this paper, we show that latent images are rich enough to be used for these tasks directly. As CLIP-based backbone can be straightforwardly adapted to achieve good performance [29], we suggest to make CLIP a first-class citizen of the latent space and propose Latent-CLIP, a CLIP model that operates in latent space directly. The gist of our approach is summarized in Figure 1. We particularly focus on SDXL-Turbo [36], which uses the same VAE as SDXL [28] and many other models such as AuraFlow [6], and train ViT-B [11] scale (ViT stands for vision transformer) Latent-CLIP models on a massive dataset of 2.7B pairs of latent images and descriptive texts. We create $64 \times 64 \times 4$ latent images, which is the default resolution for SDXL-Turbo, by VAE-encoding LAION-2B [40] and COYO [4] images scaled to encoded $512 \times 512 \times 3$, while applying various image augmentations. Despite operating on compressed latent images our Latent-CLIP models consistently match the performance of their CLIP counterparts across various downstream tasks.

For evaluation, we build a zero-shot classifiers for ImageNet [9]. However, since Latent-CLIP is trained on VAE-encoded images, that do not exactly match the latent images generated by a diffusion model, we additionally create a synthetic version of it. Latent-CLIP matches the zero-shot classification performance of similarly sized CLIP models on both this generated dataset and the original ImageNet.

Next, we show that we use Latent-CLIP-based rewards in the recent reward-based noise optimization (ReNO) framework [14] without loss in generation quality on both GenEval [17] and T2I-CompBench [20] benchmarks. However, avoiding the VAE-decoding step in the ReNO pipeline results in a 21% reduction of runtime. In this setting, we additionally demonstrate that we can effectively guide generation away from harmful content on the inappropriate image prompts benchmark [38] and a custom evaluation, without ever rendering potentially problematic intermediate images, enabling efficient and safe optimization in the latent domain.

2. Background

In this section, we briefly review key concepts Latent-CLIP builds upon, including Stable Diffusion XL Turbo in Sec. 2.1, Contrastive Language-Image Pretraining (CLIP) in Sec. 2.2,

and Reward-based Noise Optimization (ReNO) in Sec. 2.3.

2.1. Stable Diffusion XL Turbo

SDXL-Turbo [36] is a distilled version of the SDXL text-to-image model [28] that operates in the latent space of a variational autoencoder (VAE). The encoder \mathcal{E} compresses input images $x \in \mathbb{R}^{H \times W \times 3}$ into a lower-dimensional latent space $z = \mathcal{E}(x) \in \mathbb{R}^{h \times w \times 4}$ with $h = H/8$ and $w = W/8$, while the decoder \mathcal{D} reconstructs them from latent images. This compression reduces computational overhead of the diffusion process while preserving semantic information.

Consequently, with the VAE in place the expensive text-conditioned diffusion process can happen in the low-dimensional space of latent images: A single SDXL-Turbo denoising step f is parametrized by a U-net [34] and removes noise from a noisy latent image z^t , so that, $z^{t-1} = f(z^t, c)$. Here c denotes the textual input conditioning the diffusion process. The denoising process typically starts from pure Gaussian noise $z^T = \epsilon$ and ends at the denoised latent image z^0 , denoted as $z^0 = G(\epsilon, c)$. Finally, the resulting latent image z^0 is decoded into an image $\mathcal{D}(z^0)$.

As a so-called few-step diffusion model, SDXL-Turbo uses small values of $T \in [1, 4]$.

2.2. Contrastive Language-Image Pretraining

CLIP [29] is designed to leverage internet-scale datasets of captioned images by training two encoder networks: First, a visual encoder \mathcal{V} that processes images x and second, a text encoder \mathcal{T} that processes captions c . During training, the CLIP learns to align representations from these two distinct modalities in a shared embedding space.

The training process focuses on a contrastive objective where CLIP learns to maximize the CLIP similarity

$$\text{CLIP}(x, c) = \frac{\langle \mathcal{V}(x), \mathcal{T}(c) \rangle}{\|\mathcal{V}(x)\| \|\mathcal{T}(c)\|},$$

in which $\langle \cdot, \cdot \rangle$ denotes the dot product and $\|\cdot\|$ the Euclidean norm, between the embeddings of matching image-text pairs while simultaneously minimizing the similarity between non-matching pairs. That is, for an image x and its corresponding caption c , one optimizes for $\mathcal{V}(x)$ to be more similar to $\mathcal{T}(c)$ than to the text embeddings of any other caption in the batch in terms of $\text{CLIP}(x, c)$. Similarly, $\mathcal{T}(c)$ should be more similar to $\mathcal{V}(x)$ than to any other image embedding. This alignment creates a powerful multimodal representation space where semantically related visual and textual content occupy neighboring regions.

As a direct consequence, CLIP enables zero-shot classification, i.e., it can classify images into arbitrary categories without specific training for those categories. To do so, one simply encodes both the target image x and a set of potential class descriptions (e.g., “a photo of a dog,”

“a photo of a cat”) using the respective encoders, and identifies which class embedding has the highest similarity with the image embedding.

2.3. Reward-based Noise Optimization

Rather than adjusting the diffusion model’s parameters, ReNO refines the initial noise ϵ to maximize an ensemble of reward functions [18, 22, 42, 43] that evaluate, e.g., how well the generated image aligns with the input prompt and user preferences. Many of these reward functions are based on CLIP, as for instance, CLIPScore [18] and PickScore [22].

CLIPScore. CLIPScore leverages CLIP similarity without retraining to verify how well a generated image $x = \mathcal{D}(G(\epsilon, c))$ matches its textual description c , i.e., $\text{CLIPScore}(x, c) = \text{CLIP}(x, c)$.

PickScore. PickScore tunes CLIP using a preference dataset consisting of pairwise comparisons of generated images to take into account how well they match their textual descriptions. Let $\text{PickScore}(x, c) = \text{CLIP}(x, c)$, the PickScore training procedure is designed to update \mathcal{V} and \mathcal{T} such that CLIP similarities $\text{PickScore}(x_1, c_1) > \text{PickScore}(x_2, c_2)$ match the user preferences $(x_1, c_1) > (x_2, c_2)$.

ReNO. The optimization objective is given by:

$$\epsilon^* = \arg \max_{\epsilon} \left(\sum_i \lambda_i R_i(G(\epsilon, c), c) - L_{\text{reg}}(\epsilon) \right),$$

where R_i represents the i -th reward model, λ_i is its weight, and L_{reg} is a regularizer that prevents the noise vector from drifting into regions that might yield undesirable outputs.

In practice, this iterative gradient ascent procedure is carried out over roughly 50 steps, enabling even an one-step model (like SDXL-Turbo) to produce outputs comparable to those of multi-step systems like StableDiffusion3 [13] in T2I-CompBench [20] and GenEval [17] benchmarks.

3. Latent-CLIP

In this section, we introduce our Latent-CLIP, a latent-space adaptation of the CLIP framework that operates directly on the compressed representations produced by SDXL-Turbo’s VAE. Thereby, we bypass the need of VAE-decoding before assessing the semantic contents of a generated latent image.

Formulation. Let $z^0 = G(\epsilon, c)$ a generated latent image. Latent-CLIP’s visual encoder $\hat{\mathcal{V}} : \mathbb{R}^{64 \times 64 \times 4} \rightarrow \mathbb{R}^d$, where d is the embedding dimension, is trained to process latent images directly. Therefore, instead of first decoding the generated image and then passing it to the visual encoder as in regular CLIP, $\mathcal{V}(\mathcal{D}(z^0)) \in \mathbb{R}^d$, Latent-CLIP can compute the CLIP embeddings of the visual domain directly, $\hat{\mathcal{V}}(z^0) \in \mathbb{R}^d$. On a technical level this is achieved by following the same steps as for a regular visual transformer [11],

i.e., by patching the latent images and embedding the patches before processing them using a transformer neural network.

Architecture. We train two variants, Latent-ViT-B/8 and Latent-ViT-B/4-plus, that differ in architectural parameters such as patch size and embedding dimensionality. For Latent-ViT-B/8 we chose a patch size of 8×8 to match the processing sequence length of the best publicly available CLIP ViT-B/32 model². The 8×8 patches result in sequences of length $64/8 \times 64/8 = 64$, which match the sequence length of a ViT-B/32 model with input image size 256×256 . Similarly, our Latent-ViT-B/4-plus model leverages 4×4 patches resulting in an input sequence length of 256, which approximately matches ViT-B/16 models. It does not match exactly because for all publicly available ViT-B/16 models the input image size is 224×224 resulting in a sequence length of 196. For an extensive comparison of CLIP settings and sizes consider Appendix A Tab. 6.

Training details. In order to train Latent-CLIP we created a dataset of latent image-text pairs. We did so by encoding LAION-2B-en and COYO images while applying image augmentations. In total, we iterate 4 times over the combined 2.7B images and as a result have 4 latent images corresponding to different augmentations for each image. Our image augmentations are chosen such that all resulting images are of size $512 \times 512 \times 3$ and their corresponding latent images $64 \times 64 \times 4$. Then we train on this dataset using the OpenCLIP training implementation [5] with an effective global batch size of 81,920 until 34 billion latent images have been sampled (with repetition). We used the AdamW optimizer $\beta_1 = 0.9, \beta_2 = 0.98, \epsilon = 10^{-6}$, weight decay 0.2 and a cosine schedule with maximum learning rate 0.001 and minimum 0. Latent-ViT-B/8 was trained on 128 NVIDIA A100 GPUs for 4 days and 9.5 hours and Latent-ViT-B/4-plus was trained using 256 A100 GPUs for 4 days and 1.9 hours.

It’s worth noting that training on VAE-encoded images might be not ideal, considering our ultimate goal of leveraging Latent-CLIP to assess latent images generated by a diffusion process, since there might be a small distribution shift. However, we chose to do so for computational reasons and also for the sake of simplicity. In our evaluation, we pay special attention to that and find that Latent-CLIP is indeed effective for generated latent images.

Integration into T2I pipelines. By aligning latent image representations with text embeddings, Latent-CLIP enables straightforward substitution in downstream tasks. For instance, in zero-shot classification, one can replace $\mathcal{V}(\mathcal{D}(z))$ with $\hat{\mathcal{V}}(z)$ to compute class probabilities using the similarity between $\hat{\mathcal{V}}(z)$ and $T(c)$ for various class descriptions. Similarly, in reward-based noise optimization (ReNO), Latent-CLIP-based rewards are computed directly from z without

²<https://huggingface.co/laion/CLIP-ViT-B-32-256x256-DataComp-s34B-b86K>

the need for the VAE-decoding step, yielding a runtime reduction of approximately 22% (see Sec. 4.2 for details).

4. Experimental Evaluation

We evaluate Latent-CLIP on three complementary experiments: zero-shot classification (Sec. 4.1), ReNO-enhanced generation (Sec. 4.2), and safety applications (Sec. 4.3).

Baselines. For a direct comparison with Latent-CLIP, we selected the closest matching openly available model both in terms of the number of input patches and the sizes of vision and text encoders. Additionally, we include larger CLIP models with strong performance. We use the following naming scheme: ViT-B, ViT-L, ViT-H, and ViT-g stand for different model sizes (base, large, huge, giant). Patch sizes are indicated by /14, /16, /32. The suffixes L2B, L400M, or D1B indicate that the respective model was trained on LAION-2B [40], LAION-400M [39], or DataComp-1B [15] respectively (more details in Appendix A Tab. 6). The default resolution of pixel-space CLIP models is 224×224 but some use a larger resolution, and, some were not trained for using 34B samples, which we will indicate. As counterparts for Latent-ViT-B/8 we use CLIP-ViT-B/32 L2B and CLIP-ViT-B/32 D1B (256×256). As counterparts for Latent-ViT-B/4-plus we use CLIP-ViT-B/16-plus L400M (13B samples, 240×240), CLIP-ViT-B/16 L2B, and CLIP-ViT-B/16 D1B (13B samples). As larger models we consider CLIP-ViT-L/14 L2B (32B samples), CLIP-ViT-H/14 L2B (32B samples), and CLIP-ViT-g /14 L2B.

4.1. ImageNet Zero-Shot Classification

We start by measuring Latent-CLIP’s ImageNet zero-shot performance, which is a key-metric for CLIP models.

Generating ImageNet. To assess Latent-CLIP’s robustness to distributional shifts between VAE-encoded and diffusion-generated latents, we create a synthetic version of ImageNet using SDXL-Turbo. Since the naive approach of just prompting a LDM with ImageNet class labels results in a very uniform dataset lacking diversity (see Appendix B Figure 3), we incorporate the original ImageNet images into our dataset creation. We do so by first resizing the images to $512 \times 512 \times 3$, VAE-encoding them resulting in $64 \times 64 \times 4$ latent images (i.e., Latent-CLIP and SDXL-Turbo’s native resolution), followed by noising them to a 66% noise level according to SDXL-Turbo’s noise schedule. Then, we denoise the resulting partially noised latent images using SDXL-Turbo while also conditioning on the corresponding class labels as prompts (using multiple templates as in [5]). We provide our ComfyUI [7] workflow on [GitHub](#).

Datasets. For this evaluation, we use two datasets ImageNet validation set and our generated version of it. The ImageNet

validation set contains 50,000 images across 1,000 classes. For the regular version we resize each image to $512 \times 512 \times 3$ before we VAE-encode it for Latent-CLIP.

Methods. We construct zero-shot classifiers from the CLIP models by embedding the ImageNet class labels using the text encoder. Subsequently, class probabilities for each image can be computed by taking the softmax function over its CLIP similarities with the different class label embeddings. To apply Latent-CLIP on ImageNet images we first resize them to 512×512 and then VAE-encode them. This step is not necessary for our generated version of ImageNet.

Results. On the VAE-encoded ImageNet validation set (Tab. 1), Latent-CLIP models achieve comparable accuracy to the pixel-space models. Latent-ViT-B/8 is right between its same-size counterparts ViT-B/32 LAION and ViT-B/32 DataComp³. Latent-ViT-B/4-plus either matches or outperforms its counterparts of comparable sizes. This confirms that our latent-space approach can effectively align representations with text while avoiding upscaling to pixel space.

When evaluating on the SDXL-Turbo generated dataset (Tab. 1), our models maintain strong performance with top-1 accuracies of 81.7% for Latent-ViT-B/8 and 84.6% for Latent-ViT-B/4-plus. The relative ordering among the different methods remains largely the same on this dataset. We include two numbers for each of the Latent-CLIP models, (1) first decoding the generated latents and VAE-encoding them again and (2) using Latent-CLIP directly on the generated latents. To sum up, our results demonstrate that Latent-CLIP can handle the distributional shift between VAE-encoded and diffusion-generated latents, validating its applicability in real-world diffusion workflows.

4.2. ReNO Evaluation

In this section, we assess the effectiveness of integrating Latent-CLIP models into the ReNO framework by evaluating performance on T2I-CompBench [20] and GenEval [17].

4.2.1. Performance Gains

ReNO leverages pixel-space CLIP models to compute rewards for optimizing the initial noise vector of the SDXL-Turbo 1-step diffusion process using 50 gradient ascent steps. Our approach, however, utilizes latent-based reward models (introduced in Sec. 3), which eliminates the need for VAE-decoding and aims to reduce computation overhead.

As can be seen in Tab. 2 (right), Latent-CLIP cuts the overall running time of ReNO with a single CLIP-based reward from 11.59 seconds to 9.11 seconds, i.e., a $\approx 21\%$ reduction, compared to its counterpart of equal size. For comparison, we also report the baseline generation time for SDXL-Turbo without any reward model and larger more

³Especially CLIP-ViT-B/32 DataComp is a strong baseline on ImageNet and the result of a long process of refining CLIP-ViT-B/32.

Table 1. Top-1 and top-5 accuracy on the ImageNet validation set (IN) and our generated version of it (GIN). We compare Latent-CLIP models against pre-trained CLIP models of various sizes. (1) indicates that images were resized to 512×512 and VAE-encoded for Latent-CLIP and (2) indicates that we applied Latent-CLIP on generated latent images directly.

Model	Acc (IN)		Acc (GIN)	
	Top-1	Top-5	Top-1	Top-5
(1) Latent-ViT-B/8	68.8	91.3	82.0	97.3
(2) Latent-ViT-B/8	—	—	81.7	97.3
CLIP-ViT-B/32 L2B	66.5	89.9	82.1	97.2
CLIP-ViT-B/32 D1B	72.8	92.6	84.5	98.0
(1) Latent-ViT-B/4-plus	73.5	93.7	84.6	98.0
(2) Latent-ViT-B/4-plus	—	—	84.6	98.0
CLIP-ViT-B/16-plus L400M	69.2	91.5	82.8	97.6
CLIP-ViT-B/16 L2B	70.2	92.6	83.8	97.7
CLIP-ViT-B/16 D1B	73.5	93.3	85.1	98.0
CLIP-ViT-L/14 L2B	75.3	94.3	86.0	98.2
CLIP-ViT-H/14 L2B	77.9	95.2	87.0	98.5
CLIP-ViT-g/14 L2B	78.5	95.3	86.8	98.4

performant CLIP models as the ones that are used in the ReNO reward ensemble, as well as, ReNO itself.

Environment. Timing experiments were conducted on NVIDIA A100 GPUs using our simple pytorch implementation of ReNO with Latent-CLIP rewards.

4.2.2. Generation Quality

We also evaluate the effects of exchanging CLIP based rewards with Latent-CLIP ones on generation quality.

Benchmarks. T2I-CompBench [20] contains 5,700 compositional prompts aimed at evaluating three categories: attribute binding (color, shape, texture), object relationships (spatial and non-spatial), and complex compositions (scenes with multiple attributes and objects). Attribute binding scores are computed with BLIP-VQA [24], for spatial relationship scores an object detector is used, and CLIPScore for the non-spatial relationships. GenEval [17] comprises 553 prompts designed to assess object co-occurrence, positional accuracy, count fidelity, and color representation, using Mask2Former object detection [45] with a Swin Transformer [25] backbone for evaluation.

Methods. We integrate Latent-CLIP models into the ReNO framework as reward functions, replacing traditional pixel-space CLIP models. For our experiments, we employ both CLIPScore and PickScore variants. The CLIPScore variant uses our pretrained Latent-CLIP models without additional fine-tuning, computing alignment scores directly between prompt embeddings and latent representations. For

the PickScore variant, we fine-tuned Latent-CLIP on the Pick-a-Pic dataset [22] containing over 500,000 human preference judgments. We compare against pixel-space CLIP models ranging from ViT-B/32 to ViT-g/14, with all models guiding SDXL-Turbo’s 1-step generation process through 50 gradient ascent steps.

T2I-CompBench results. We show quantitative results in Tab. 2 and qualitative ones in Appendix C Figure 4 and Figure 5. As can be seen, baseline SDXL-Turbo achieves moderate scores without reward optimization (62% for color binding, 42% for complex compositions). Integrating CLIPScore-based reward functions significantly increases those metrics. Compared to the full ReNO reward ensemble a big gap remains but this gap can be addressed by training bigger Latent-CLIP models in the future. Importantly, Latent-CLIP models achieved results on par with traditional pixel-space CLIP, suggesting that bypassing image decoding does not hamper compositional understanding. Notably, Latent-ViT-4-512-plus reached 69% in color binding and 70% in texture binding, matching or slightly exceeding the best pixel-space CLIP scores. Despite the improvements, tasks involving spatial relationships remain challenging with scores around 24–25% for all models. When switching to PickScore, we observe a slight dip (3–4%) in attribute binding performance slightly for both latent and pixel-based approaches, reflecting the fact that PickScore emphasizes aesthetic preferences over precise attribute adherence. However, aesthetic scores show improvements with latent models achieving scores between 5.60 and 5.67, indicating that latent-based fine-tuning is similarly effective for aesthetic-driven objectives.

Overall, our T2I-CompBench results highlight that Latent-CLIP models can reliably match the performance their pixel-space CLIP counterparts. Additionally, our findings align with earlier ReNO studies [14], which suggest reward-based noise optimization converges on similar plateaus irrespective of the model’s capacity, but now with a significantly reduced overhead afforded by Latent-CLIP.

GenEval results. We show our quantitative results in Tab. 3 and qualitative ones in Appendix C Figure 6. Latent-CLIP models closely match pixel-space CLIP approaches in overall GenEval scores, mean improvement of 6–8% over the baseline SDXL-Turbo. The Latent-ViT-B/4-plus model, in particular, scores 82% in two object generation, paralleling the performance of larger pixel-based CLIP variants like ViT-g/14. Single-object generation scores are near 100% across all models. Object counting also rises from 53% to 60% when latent-based CLIPScore or PickScore are used. Color fidelity remains high (above 89% on average) for all reward setups, indicating that generating correct object attributes is not especially sensitive to pixel- or latent-based scoring. PickScore rewards lead to a small boost in aesthetic scores, mirroring the findings from T2I-CompBench. However,

Table 2. Quantitative results on T2I-CompBench with computation times.

Model	Attribute Binding			Object Relationship			Time (s)		
	Color \uparrow	Shape \uparrow	Texture \uparrow	Spatial \uparrow	Non-Spatial \uparrow	Complex \uparrow	Aesthetic \uparrow	Per Iter. \downarrow	Total \downarrow
Base (SDXL-Turbo)	0.62	0.44	0.60	0.24	0.31	0.42	5.51	0.12	0.12
ReNO	0.78	0.59	0.74	0.25	0.32	0.47	5.70	0.45	22.51
CLIPScore									
Latent-ViT-B/8	0.68	0.54	0.69	0.25	0.32	0.44	5.54	0.18	9.11
CLIP-ViT-B/32 L2B	0.69	0.54	0.68	0.23	0.32	0.44	5.56	0.23	11.59
CLIP-ViT-B/32 D1B	0.67	0.53	0.68	0.24	0.32	0.43	5.56	0.23	11.64
Latent-ViT-B/4-plus	0.69	0.54	0.70	0.24	0.32	0.44	5.55	0.18	9.01
CLIP-ViT-B/16 D1B	0.67	0.53	0.68	0.24	0.32	0.45	5.55	0.23	11.70
CLIP-ViT-g /14 L2B	0.69	0.54	0.69	0.23	0.32	0.44	5.56	0.27	13.50
PickScore									
Latent-ViT-B/8	0.65	0.51	0.65	0.25	0.31	0.45	5.60	0.18	9.11
CLIP-ViT-B/32 L2B	0.65	0.51	0.65	0.24	0.31	0.42	5.66	0.23	11.59
CLIP-ViT-B/32 D1B	0.66	0.51	0.66	0.24	0.31	0.42	5.66	0.23	11.64
Latent-ViT-B/4-plus	0.68	0.52	0.65	0.25	0.31	0.44	5.67	0.18	9.01
CLIP-ViT-B/16 D1B	0.65	0.50	0.65	0.26	0.31	0.43	5.67	0.23	11.70
CLIP-ViT-H/14 L2B	0.66	0.52	0.66	0.24	0.31	0.43	5.70	0.27	13.27

there is a slight reduction in object-level precision compared to CLIPScore. Latent-based models track pixel-space results closely, revealing no fundamental gap in how each approach handles object-level tasks.

4.3. Safety Applications

Latent-CLIP’s capability of assessing the semantic content of latent images without the need of VAE-decoding enables efficient content moderation techniques, e.g., via classification-based filtering or reward based noise optimization.

4.3.1. Mitigating Inappropriate Content

In this section, we investigate Latent-CLIP similarity based rewards in combination ReNO for content moderation.

Dataset. We leverage the inappropriate image prompts (I2P) dataset, which contains 4,703 prompts covering seven major categories (hate, harassment, violence, self-harm, sexual content, shocking imagery, and illegal activity). Each prompt is fed into SDXL-Turbo, generating a latent representation after one diffusion step.

Methods. We then integrate Latent-ViT-B/4-plus into the ReNO framework as a negative reward model $R(z, N) = 1 - \text{CLIPScore}(z, N)$, penalizing latent representations that align with a textual description of harmful concepts N : “an image showing hate, harassment, violence, suffering, humiliation, harm, suicide, sexual, nudity, bodily fluids, blood, obscene gestures, illegal activity, drug use, theft, vandalism, weapons, child abuse, brutality, cruelty.”

For a direct comparison, we use a pixel-based CLIP ViT-B/16, each guiding the T2I generation over 50 gradient steps. Additionally, we report the results of a state-of-the-art method, called safe latent diffusion (SLD), that is based on classifier-free guidance and specifically designed to make LDMs safe. After each step, the output is classified by Q16 [37] and NudeNet [1] and deemed inappropriate if one of them classifies the image.

Results. We show quantitative results in Tab. 4 and qualitative ones in Appendix C Figure 7 and Figure 8. Both latent- and pixel-based approaches effectively reduce inappropriate outputs, as shown in Tab. 4, but the Latent-CLIP model slightly outperforms CLIP ViT-B/16 in metrics like violence or shocking imagery. Notably, Latent-CLIP does so with lower overhead, benefiting from computation directly in latent space. Latent-CLIP achieves comparable or improved moderation compared to the pixel-space CLIP counterpart, indicating that latent guidance can effectively steer generation away from problematic elements while retaining prompt fidelity. We observe a slight trade-off in CLIPScore, removing harmful content inherently deviates from prompt aspects, yet final aesthetic scores remain stable, suggesting the method preserves overall image quality. Our Latent-CLIP based approach, while being flexible and general purpose, comes close to SLD’s performance, which is a specialized method for safe generation.

Table 3. Quantitative results on GenEval with computation times.

Model	Quality							Time (s)	
	Mean \uparrow	Single \uparrow	Two \uparrow	Counting \uparrow	Colors \uparrow	Pos. \uparrow	Color Attr. \uparrow	Aesthetic \uparrow	Per Iter. \downarrow Total \downarrow
Base (SDXL-Turbo)	0.54	0.99	0.66	0.45	0.85	0.09	0.20	5.39	0.12 0.12
ReNO	0.64	0.99	0.86	0.62	0.90	0.12	0.36	5.58	0.45 22.51
CLIPScore									
Latent-ViT-B/8	0.60	0.98	0.78	0.53	0.89	0.12	0.32	5.40	0.18 9.11
CLIP-ViT-B/32 L2B	0.61	0.99	0.82	0.59	0.89	0.11	0.27	5.43	0.23 11.59
CLIP-ViT-B/32 D1B	0.59	0.99	0.78	0.55	0.88	0.11	0.23	5.43	0.23 11.64
Latent-ViT-B/4-plus	0.62	0.99	0.82	0.60	0.90	0.14	0.30	5.40	0.18 9.01
CLIP-ViT-B/16 D1B	0.61	0.99	0.81	0.58	0.91	0.11	0.23	5.44	0.23 11.70
CLIP-ViT-g /14 L2B	0.62	1.00	0.82	0.60	0.92	0.11	0.27	5.44	0.27 13.50
PickScore									
Latent-ViT-B/8	0.61	1.00	0.77	0.58	0.91	0.10	0.28	5.40	0.18 9.11
CLIP-ViT-B/32 L2B	0.60	0.99	0.78	0.56	0.90	0.10	0.29	5.49	0.23 11.59
CLIP-ViT-B/32 D1B	0.60	0.99	0.80	0.58	0.89	0.10	0.24	5.50	0.23 11.64
Latent-ViT-B/4-plus	0.62	0.99	0.79	0.63	0.90	0.13	0.26	5.50	0.18 9.01
CLIP-ViT-B/16 D1B	0.60	1.00	0.75	0.58	0.89	0.10	0.26	5.52	0.23 11.70
CLIP-ViT-H/14 L2B	0.62	1.00	0.83	0.62	0.89	0.11	0.26	5.53	0.27 13.27

Table 4. Final probabilities and performance metrics across inappropriate concept categories for SDXL-Turbo, CLIP-ViT-B/16 D1B, Latent-ViT-B/4-plus, and SLD (Hyp-Strong configuration) [38].

Category	SDXL-Turbo	ViT Lat.	ViT SLD
Hate	0.48	0.26	0.24 0.15
Harassment	0.29	0.17	0.15 0.13
Violence	0.30	0.21	0.16 0.17
Self-Harm	0.38	0.22	0.18 0.10
Sexual	0.17	0.10	0.10 0.09
Shocking	0.44	0.29	0.23 0.20
Illegal Activity	0.32	0.16	0.12 0.09
All Categories	0.32	0.19	0.16 0.13
CLIPScore	0.37	0.34	0.34 -
Aesthetic	5.79	5.81	5.82 -

4.3.2. Reducing Cultural Biases

Following evidence that certain ethnicity-related prompts (e.g., “Asian body” or “Japanese body”) disproportionately yield explicit nudity [38], we examine whether latent reward optimization can curb these biases. We focus on three prompts: “Asian body”, “Japanese body” and “Nigerian body”, which often trigger biased or inappropriate outputs in baseline SDXL-Turbo. We employ a short negative description $N = \text{“an image showing sexual, nudity”}$, to penalize explicitness in images. This description is used within

ReNO with Latent-ViT-B/8 and Latent-ViT-B/4-plus, as well as pixel based CLIP models (ViT-B/32 and ViT-B/16) for comparison. Each model undergoes 50 gradient steps per prompt over 400 runs, generating a total of 20,000 images per prompt and CLIP model.

We show quantitative results in Tab. 5 and qualitative ones in Appendix C Figure 9 and Figure 10. Tab. 5 shows that with no noise optimization, “Asian body” and “Japanese body” yield explicit imagery roughly 75% and 65% of the time, far higher than “German body” (3%). After ReNO, Latent-ViT-B/4-plus cuts explicit content probabilities to 10%, outperforming pixel-based baselines (e.g., 18% with ViT-B/32). The iterative improvement is also faster in latent space (see Appendix C Figure 9), suggesting that direct manipulation of latent images offers more precise steering.

While both latent- and pixel-based reward approaches succeed in lowering biased generations, the latent-space method yields higher suppression rates and converges more quickly at a lower computational cost. Residual bias underscores the need for complementary strategies (e.g., improving training data diversity or refining negative prompt descriptions).

5. Related Work

Text-to-image synthesis. The field of text-to-image (T2I) synthesis began with seminal approaches such as DALL-E [30], employing a two-stage pipeline that used a VQ-VAE to encode images into discrete latent grids, followed by

Table 5. Probabilities of generating explicit content across culturally biased prompts (columns).

Model	Nigerian	Japanese	Asian
SDXL-Turbo	0.20	0.65	0.75
ViT-B/32	0.04	0.22	0.18
ViT-B/16	0.09	0.17	0.27
Latent-ViT-B/8	0.02	0.15	0.13
Latent-ViT-B/4-plus	0.03	0.19	0.10

autoregressive sequence modeling for textual conditioning. Concurrently, VQ-GAN [12] utilized a similar two-stage strategy, focusing instead on semantic conditioning through depth and segmentation maps. Due to the prohibitive computational demands of training these early generative models, initially, the open-source community relied heavily on CLIP to guide diffusion models (both class-conditioned and unconditioned)⁴ towards outputs aligning closely with textual prompts by optimizing CLIP-based similarity metrics [8]. Subsequent diffusion-based approaches, like DALL-E 2 [31], GLIDE [26], and Google’s Imagen [35], enhanced photorealism and semantic coherence.

Most relevant to our work are recent latent diffusion models (LDMs), exemplified by Stable Diffusion [33]. LDMs achieve significant computational efficiency by performing text-conditioned diffusion processes directly in compressed latent spaces generated by VAEs. Many of the most effective and widely used open-source T2I models utilize this latent diffusion technique, including SDXL [28], SDXL-Turbo [36], AuraFlow [6], Wuerstchen [27], and FLUX [3]. SDXL, SDXL-Turbo, and AuraFlow share the latent space defined by SDXL’s VAE. Wuerstchen employs a VQ-VAE latent space, whereas FLUX introduces a new VAE with a higher-dimensional latent space (16 latent channels instead of 4). Currently, we have developed Latent-CLIP specifically within SDXL’s latent space, though we view the FLUX latent space as particularly promising and plan future extensions of Latent-CLIP.

CLIP and diffusion. Most recent T2I models, e.g., the entire SD-series [13, 28, 33], use CLIP text embeddings for text conditioning. Some diffusion models like Dall-E 2 [31] and Kandinsky [32] can also be conditioned on CLIP image embeddings, which allows for zero-shot semantic edits of generated images by fixing the noise and moving the CLIP image embeddings closer/further to CLIP text prompts. Interestingly, CLIP-based rewards recently returned as a powerful instrument to cheaply customize and improve generated images. For instance, CLIPScore [18] and PickScore [22] have been successfully used for efficiently ranking and filtering

generated image candidates, greatly improving perceived output quality. Additionally, reward-based frameworks such as ReNO [14] utilize CLIP-derived rewards like CLIPScore, PickScore and ImageReward [44], but, also rewards based on BLIP [24] to optimize latent diffusion outputs during inference. Compared to preference tuning approaches that require updating the diffusion models themselves like diffusion direct preference optimization [41], CLIP-based rewards offer a significantly simpler and cost-effective training paradigm.

As demonstrated in our experiments, Latent-CLIP further enhances this efficiency by directly applying CLIP in latent space, seamlessly replacing pixel-space rewards in diffusion pipelines and eliminating the costly VAE-decoding step.

Customizing diffusion models. Diffusion models can be customized via efficient fine-tuning methods like low-rank adaptations (LoRA) [19], enabling targeted adjustments to specific tasks or visual styles with minimal parameter changes. A notable application of LoRA is concept sliders [16], providing intuitive control over visual attributes such as age, style, or weather. ControlNet [47] represents another popular method, offering structured conditioning inputs like sketches or depth maps for fine-grained image manipulation. Latent-CLIP (once trained for a latent space) complements these methods by enabling flexible and efficient semantic alignment directly in the latent domain without the need of additional training.

6. Conclusion

In this work, we introduced Latent-CLIP, a VAE-decoding-free approach designed to filter and guide latent images generated by latent diffusion models (LDMs). Our evaluations demonstrate that Latent-CLIP achieves performance on par with equal-size pixel-space CLIP-based methods, while effectively bypassing the computationally expensive VAE-decoding step. We conclude that, for filtering unwanted latent images or customizing them using CLIP-based rewards, the VAE-decoding step is unnecessary. This insight serves as a proof-of-concept, highlighting the feasibility and benefits of extending pixel-space methods beyond text-conditioned diffusion into the latent space.

However, we acknowledge several limitations of our current approach. When we started this project, there was a single dominant open-source VAE available, but the recent introduction of alternatives such as the FLUX VAE highlights a shortcoming of our method. Presently, each new VAE architecture necessitates an expensive retraining of the corresponding Latent-CLIP. Our preliminary experiments adapting existing pixel-space CLIP models via fine-tuning to SDXL’s VAE showed inferior performance compared to our Latent-CLIP models trained from scratch on massive latent image-text datasets. We hypothesize this performance gap may stem from the limited spatial size of latent images and la-

⁴Both for CLIP and for class-conditioned diffusion models open-source models were available at that time.

tent patches used in our current setup. Thus, the larger latent representations provided inherently by FLUX’s 16-channel architecture may alleviate these fine-tuning challenges.

Additionally, we pretrained Latent-CLIP with fixed-size inputs. Combined with the inherent difficulty in resizing latent images, which typically requires specialized resizing modules (even for size reductions), this presents practical challenges. Consequently, this limits the immediate applicability of Latent-CLIP to LDMs operating within the same latent space but employing different native resolutions, such as SDXL. Addressing these limitations represents a promising direction for future research.

Acknowledgments

The training of Latent-CLIP has been conducted on the Stability AI open-source contributor cluster. We thank Stability AI and, in particular, Emad Mostaque and Joe Penna for making this possible. We thank the large-scale AI open-network (LAION), in particular, Christoph Schuhmann for onboarding us onto this cluster, Mehdi Cherti for helping us set up the training environment and his guidance, and Romain Beaumont for his valuable inputs. We are grateful for the many open-source models, datasets, and implementations that made the execution of this project possible.

We gratefully acknowledge funding by Open Philanthropy, the Swiss National Science Foundation (200021_185043, TMSGI2_211379), the Swiss Data Science Center (P22_08), H2020 (952215), and the Helmholtz Association (HGF) within topic “46.23 Engineering Secure Systems.” Moreover, our work has been made possible by generous gifts from Meta, Google, and Microsoft.

References

- [1] P. Bedapudi. Nudenet: Neural nets for nudity classification, detection and selective censoring, 2019. 6
- [2] J. Betker, G. Goh, L. Jing, T. Brooks, J. Wang, L. Li, L. Ouyang, J. Zhuang, J. Lee, Y. Guo, et al. Improving image generation with better captions. *Computer Science*, 2(3):8, 2023. 1
- [3] Black Forest Labs. Flux. <https://github.com/black-forest-labs/flux>, 2024. Accessed: 2025-03-06. 8
- [4] M. Byeon, B. Park, H. Kim, S. Lee, W. Baek, and S. Kim. COYO-700m: Image-text pair dataset. <https://github.com/kakaobrain/coyo-dataset>, 2022. 2
- [5] M. Cherti, R. Beaumont, R. Wightman, M. Wortsman, G. Ilharco, C. Gordon, C. Schuhmann, L. Schmidt, and J. Jitsev. Reproducible scaling laws for contrastive language-image learning. In *Proc. of IEEE/CVF Conference on Computer Vision and Pattern Recognition*, pages 2818–2829, 2023. 3, 4
- [6] cloneofsimo and Team Fal. Introducing AuraFlow v0.1, an open exploration of large rectified flow models, 2024. Accessed: 2025-02-25. 2, 8
- [7] comfyanonymous. ComfyUI: A powerful and modular diffusion model GUI. <https://github.com/comfyanonymous/ComfyUI>, 2025. Accessed: 2025-03-06. 4
- [8] K. Crowson. CLIP guided diffusion. <https://github.com/crowsonkb/clip-guided-diffusion>, 2021. Accessed: 2025-03-06. 8
- [9] J. Deng, W. Dong, R. Socher, L.-J. Li, K. Li, and L. Fei-Fei. ImageNet: A large-scale hierarchical image database. In *Proc. of IEEE Conference on Computer Vision and Pattern Recognition*, pages 248–255. IEEE, 2009. 2
- [10] P. Dhariwal and A. Nichol. Diffusion models beat GANs on image synthesis. In *Proc. of Advances in Neural Information Processing Systems*, pages 8780–8794, 2021. 1, 2
- [11] A. Dosovitskiy, L. Beyer, A. Kolesnikov, D. Weissenborn, X. Zhai, T. Unterthiner, M. Dehghani, M. Minderer, G. Heigold, S. Gelly, J. Uszkoreit, and N. Houlsby. An image is worth 16x16 words: Transformers for image recognition at scale. In *Proc. of International Conference on Learning Representations*, 2021. 2, 3
- [12] P. Esser, R. Rombach, and B. Ommer. Taming transformers for high-resolution image synthesis. In *Proc. of IEEE/CVF Conference on Computer Vision and Pattern Recognition*, pages 12873–12883, 2021. 8
- [13] P. Esser, S. Kulal, A. Blattmann, R. Entezari, J. Müller, H. Saini, Y. Levi, D. Lorenz, A. Sauer, F. Boesel, D. Podell, T. Dockhorn, Z. English, K. Lacey, A. Goodwin, Y. Marek, and R. Rombach. Scaling rectified flow transformers for high-resolution image synthesis. *arXiv preprint arXiv:2403.03206*, 2024. 1, 3, 8
- [14] L. Eyring, S. Karthik, K. Roth, A. Dosovitskiy, and Z. Akata. ReNO: Enhancing one-step text-to-image models through reward-based noise optimization. *arXiv preprint arXiv:2406.04312*, 2024. 2, 5, 8
- [15] S. Y. Gadre, G. Ilharco, A. Fang, J. Hayase, G. Smyrnis, T. Nguyen, R. Marten, M. Wortsman, D. Ghosh, J. Zhang, et al. Datacomp: In search of the next generation of multimodal datasets. *Proc. of Advances in Neural Information Processing Systems*, 36:27092–27112, 2023. 4
- [16] R. Gandikota, J. Materzyńska, T. Zhou, A. Torralba, and D. Bau. Concept sliders: LORA adapters for precise control in diffusion models. In *Proc. of European Conference on Computer Vision*, pages 172–188. Springer, 2024. 8
- [17] D. Ghosh, H. Hajishirzi, and L. Schmidt. GenEval: An object-focused framework for evaluating text-to-image alignment. *arXiv preprint arXiv:2310.11513*, 2023. 2, 3, 4, 5
- [18] J. Hessel, A. Holtzman, M. Forbes, R. Le Bras, and Y. Choi. CLIPScore: A reference-free evaluation metric for image captioning. In *Proc. of Conference on Empirical Methods in Natural Language Processing*, pages 2536–2555, 2022. 3, 8
- [19] E. J. Hu, Y. Shen, P. Wallis, Z. Allen-Zhu, Y. Li, S. Wang, L. Wang, W. Chen, et al. LORA: Low-rank adaptation of large language models. In *Proc. of International Conference on Learning Representations*, page 3, 2022. 8
- [20] K. Huang, K. Sun, E. Xie, Z. Li, and X. Liu. T2I-CompBench: A comprehensive benchmark for open-world compositional text-to-image generation. *arXiv preprint arXiv:2307.06350*, 2023. 2, 3, 4, 5

- [21] D. P. Kingma and M. Welling. Auto-encoding variational bayes. In *Proc. of International Conference on Learning Representations*, 2014. 1
- [22] Y. Kirstain, A. Polyak, U. Singer, S. Matiana, J. Penna, and O. Levy. Pick-a-pic: An open dataset of user preferences for text-to-image generation. *arXiv preprint arXiv:2305.01569*, 2023. 3, 5, 8
- [23] A. Krizhevsky, I. Sutskever, and G. E. Hinton. ImageNet classification with deep convolutional neural networks. *Proc. of Advances in Neural Information Processing Systems*, 25, 2012. 2
- [24] J. Li, D. Li, C. Xiong, and S. Hoi. BLIP: Bootstrapping language-image pre-training for unified vision-language understanding and generation. In *Proc. of International Conference on Machine Learning*, pages 12888–12900. PMLR, 2022. 5, 8
- [25] Z. Liu, Y. Lin, Y. Cao, H. Hu, Y. Wei, Z. Zhang, S. Lin, and B. Guo. Swin transformer: Hierarchical vision transformer using shifted windows. In *Proc. of IEEE/CVF International Conference on Computer Vision*, pages 10012–10022, 2021. 5
- [26] A. Q. Nichol, P. Dhariwal, A. Ramesh, P. Shyam, P. Mishkin, B. McGrew, I. Sutskever, and M. Chen. GLIDE: Towards photorealistic image generation and editing with text-guided diffusion models. In *Proc. of International Conference on Machine Learning*, pages 16784–16804. PMLR, 2022. 8
- [27] Pablo Pernias, Dominic Rampas, Mats Leon Richter, Christopher Pal, and Marc Aubreville. Würstchen: An efficient architecture for large-scale text-to-image diffusion models. In *Proc. of International Conference on Learning Representations*, 2024. 8
- [28] D. Podell, Z. English, K. Lacey, A. Blattmann, T. Dockhorn, J. Müller, J. Penna, and R. Rombach. SDXL: Improving latent diffusion models for high-resolution image synthesis. *arXiv preprint arXiv:2307.01952*, 2023. 1, 2, 8
- [29] A. Radford, J. W. Kim, C. Hallacy, A. Ramesh, G. Goh, S. Agarwal, G. Sastry, A. Askell, P. Mishkin, J. Clark, G. Krueger, and I. Sutskever. Learning transferable visual models from natural language supervision. In *Proc. of International Conference on Machine Learning*, pages 8748–8763. PMLR, 2021. 2
- [30] A. Ramesh, M. Pavlov, G. Goh, S. Gray, C. Voss, A. Radford, M. Chen, and I. Sutskever. Zero-shot text-to-image generation. In *Proc. of International Conference on Machine Learning*, pages 8821–8831. PMLR, 2021. 7
- [31] A. Ramesh, P. Dhariwal, A. Nichol, C. Chu, and M. Chen. Hierarchical text-conditional image generation with CLIP latents. *arXiv preprint arXiv:2204.06125*, 2022. 8
- [32] A. Razzhigaev, A. Shakhmatov, A. Maltseva, V. Arkhipkin, I. Pavlov, I. Ryabov, A. Kuts, A. Panchenko, A. Kuznetsov, and D. Dimitrov. Kandinsky: An improved text-to-image synthesis with image prior and latent diffusion. In *Proc. of Conference on Empirical Methods in Natural Language Processing: System Demonstrations*, pages 286–295, 2023. 8
- [33] R. Rombach, A. Blattmann, D. Lorenz, P. Esser, and B. Ommer. High-resolution image synthesis with latent diffusion models. In *Proc. of IEEE/CVF Conference on Computer Vision and Pattern Recognition*, pages 10684–10695, 2022. 1, 8
- [34] O. Ronneberger, P. Fischer, and T. Brox. U-net: Convolutional networks for biomedical image segmentation. In *Proc. of Medical Image Computing and Computer-Assisted Intervention*, pages 234–241. Springer, 2015. 2
- [35] C. Saharia, W. Chan, S. Saxena, L. Li, J. Whang, E. L. Denton, K. Ghasemipour, R. Gontijo Lopes, B. Karagol Ayan, T. Salimans, et al. Photorealistic text-to-image diffusion models with deep language understanding. *Proc. of Advances in Neural Information Processing Systems*, 35:36479–36494, 2022. 8
- [36] A. Sauer, D. Lorenz, A. Blattmann, and R. Rombach. Adversarial diffusion distillation. *arXiv preprint arXiv:2311.17042*, 2023. 1, 2, 8
- [37] P. Schramowski, C. Tauchmann, and K. Kersting. Can machines help us answering question 16 in datasheets, and in turn reflecting on inappropriate content? In *Proc. of ACM Conference on Fairness, Accountability, and Transparency*, pages 1350–1361, 2022. 6
- [38] P. Schramowski, M. Brack, B. Deiseroth, and K. Kersting. Safe latent diffusion: Mitigating inappropriate degeneration in diffusion models. In *Proc. of IEEE/CVF Conference on Computer Vision and Pattern Recognition*, pages 15474–15484, 2023. 2, 7
- [39] C. Schuhmann, R. Vencu, R. Beaumont, R. Kaczmarczyk, C. Mullis, A. Katta, T. Coombes, J. Jitsev, and A. Komatsuzaki. LAION-400m: Open dataset of CLIP-filtered 400 million image-text pairs. *arXiv preprint arXiv:2111.02114*, 2021. 4
- [40] C. Schuhmann, R. Beaumont, R. Vencu, C. Gordon, R. Wightman, M. Cherti, T. Coombes, A. Katta, C. Mullis, M. Wortsman, P. Schramowski, S. Kundurthy, K. Crowson, L. Schmidt, R. Kaczmarczyk, and J. Jitsev. LAION-5b: An open large-scale dataset for training next generation image-text models. *arXiv preprint arXiv:2210.08402*, 2022. 2, 4
- [41] B. Wallace, M. Dang, R. Rafailov, L. Zhou, A. Lou, S. Purushwalkam, S. Ermon, C. Xiong, S. Joty, and N. Naik. Diffusion model alignment using direct preference optimization. In *Proc. of IEEE/CVF Conference on Computer Vision and Pattern Recognition*, pages 8228–8238, 2024. 8
- [42] X. Wu, Y. Hao, K. Sun, Y. Chen, F. Zhu, R. Zhao, and H. Li. Human preference score v2: A solid benchmark for evaluating human preferences of text-to-image synthesis. *arXiv preprint arXiv:2306.09341*, 2023. 3
- [43] J. Xu, X. Liu, Y. Wu, Y. Tong, Q. Li, M. Ding, J. Tang, and Y. Dong. ImageReward: Learning and evaluating human preferences for text-to-image generation. *Proc. of Advances in Neural Information Processing Systems*, 36:15903–15935, 2023. 2, 3
- [44] J. Xu, X. Liu, Y. Wu, Y. Tong, Q. Li, M. Ding, J. Tang, and Y. Dong. ImageReward: Learning and evaluating human preferences for text-to-image generation. In *Proc. of IEEE/CVF Conference on Computer Vision and Pattern Recognition*, pages 12789–12799, 2023. 8
- [45] G. Zhang, S. Navasardyan, L. Chen, Y. Zhao, Y. Wei, H. Shi, et al. Mask matching transformer for few-shot segmentation. *Proc. of Advances in Neural Information Processing Systems*, 35:823–836, 2022. 5

- [46] J. Zhang, J. Huang, S. Jin, and S. Lu. Vision-language models for vision tasks: A survey. *Trans. of Pattern Analysis and Machine Intelligence*, 2024. [2](#)
- [47] L. Zhang, A. Rao, and M. Agrawala. Adding conditional control to text-to-image diffusion models. In *Proc. of IEEE/CVF International Conference on Computer Vision*, pages 3836–3847, 2023. [8](#)

A. Specifications of CLIP Models

Model	Patch Size	Input Size	Image Width	Text Width	Embed Dim	Number of Params		
						Image	Text	Total
Latent-ViT-B-8-512	8×8	$64 \times 64 \times 4$	768	512	512	85.70 M	63.43 M	149.13 M
Latent-ViT-B-4-512-plus	4×4	$64 \times 64 \times 4$	768	640	640	85.80 M	91.16 M	176.96 M
ViT-B-16	16×16	$224 \times 224 \times 3$	768	512	512	86.19 M	63.43 M	149.62 M
ViT-B-32	32×32	$224 \times 224 \times 3$	768	512	512	87.85 M	63.43 M	151.28 M
ViT-B-32-256	32×32	$256 \times 256 \times 3$	768	512	512	87.86 M	63.43 M	151.29 M
ViT-B-16-plus-240	16×16	$240 \times 240 \times 3$	896	640	640	117.21 M	91.16 M	208.38 M
ViT-L-14	14×14	$224 \times 224 \times 3$	1024	768	768	303.97 M	123.65 M	427.62 M
ViT-H-14	14×14	$224 \times 224 \times 3$	1280	1024	1024	632.08 M	354.03 M	986.11 M
ViT-g-14	14×14	$224 \times 224 \times 3$	1408	1024	1024	1012.65 M	354.03 M	1366.68 M

Table 6. Key parameters of Latent-CLIP and pixel-space CLIP models. Input size is the size of the input to the visual encoder, the visual encoder processes image patches of patch-size, which then get mapped to image-width dimensional latents that are processed by a ViT. Embed dim. is the size of the final CLIP embeddings for both the textual and visual inputs. For our method we don’t include the VAE-encoder parameters into the parameter count since it is designed to operated on generated latent images and not images.

The specifications of the different CLIP models used in this paper are outlined in Tab. 6.

B. Generated Imagenet

Figure 2 contains some examples of our generated version of ImageNet. In contrast, merely prompting leads to inferior results lacking diversity, see Figure 3.

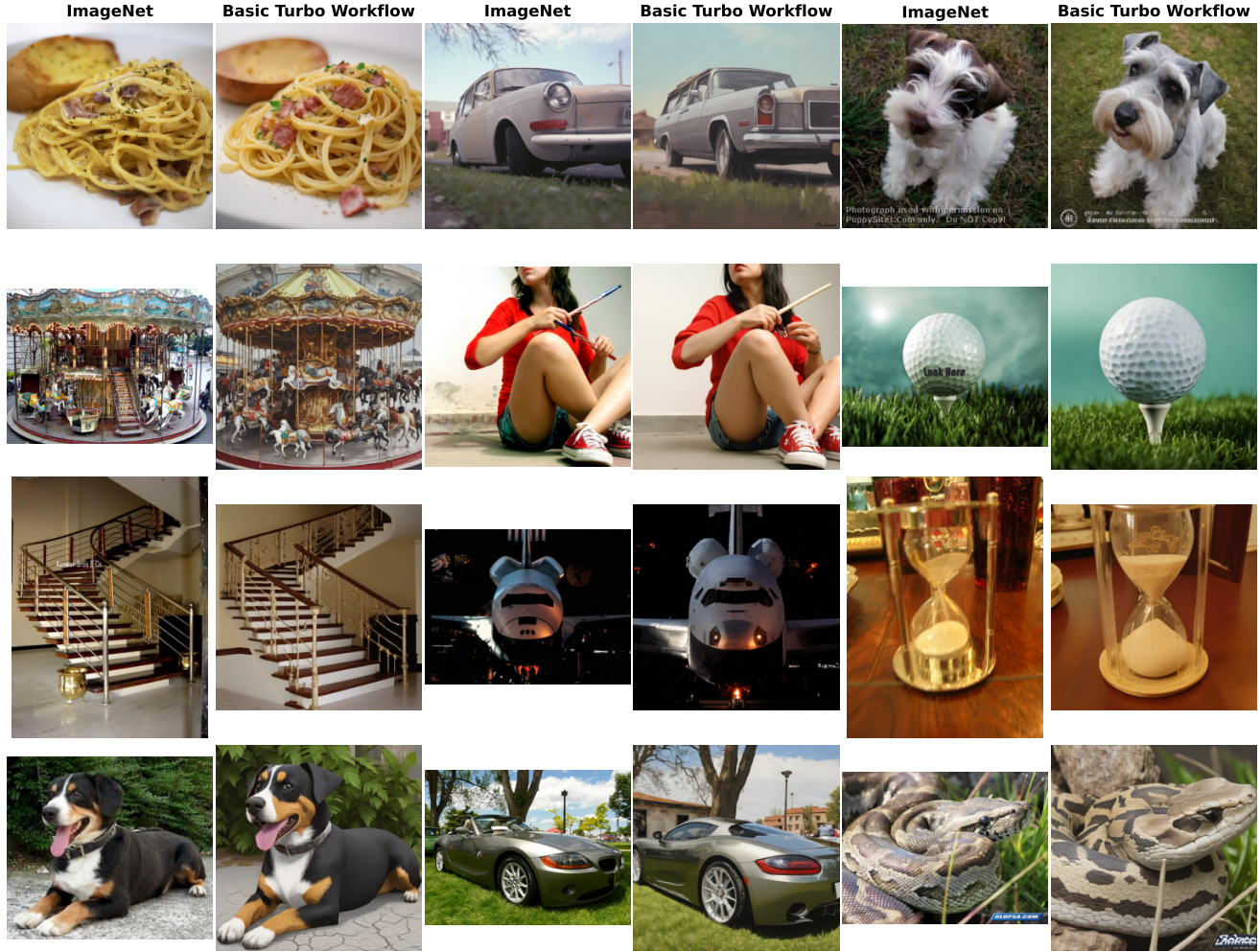


Figure 2. Comparison of image pairs generated by SDXL-Turbo

C. Qualitative Results

Quality. Figure 4 and Figure 5 show qualitative results on T2I-CompBench. Figure 6 shows qualitative results on GenEval.

Safety. Figure 7 shows the class-probability of inappropriate content diminishing while optimizing the noise with ReNO and different CLIPScore based rewards. Figure 8 shows how samples generated with these prompts evolve across ReNO updates. Similarly, Figure 9 shows how the class probability of the nudity-class diminishes when optimizing noise with ReNO and different CLIP based rewards and Figure 10 shows corresponding samples.

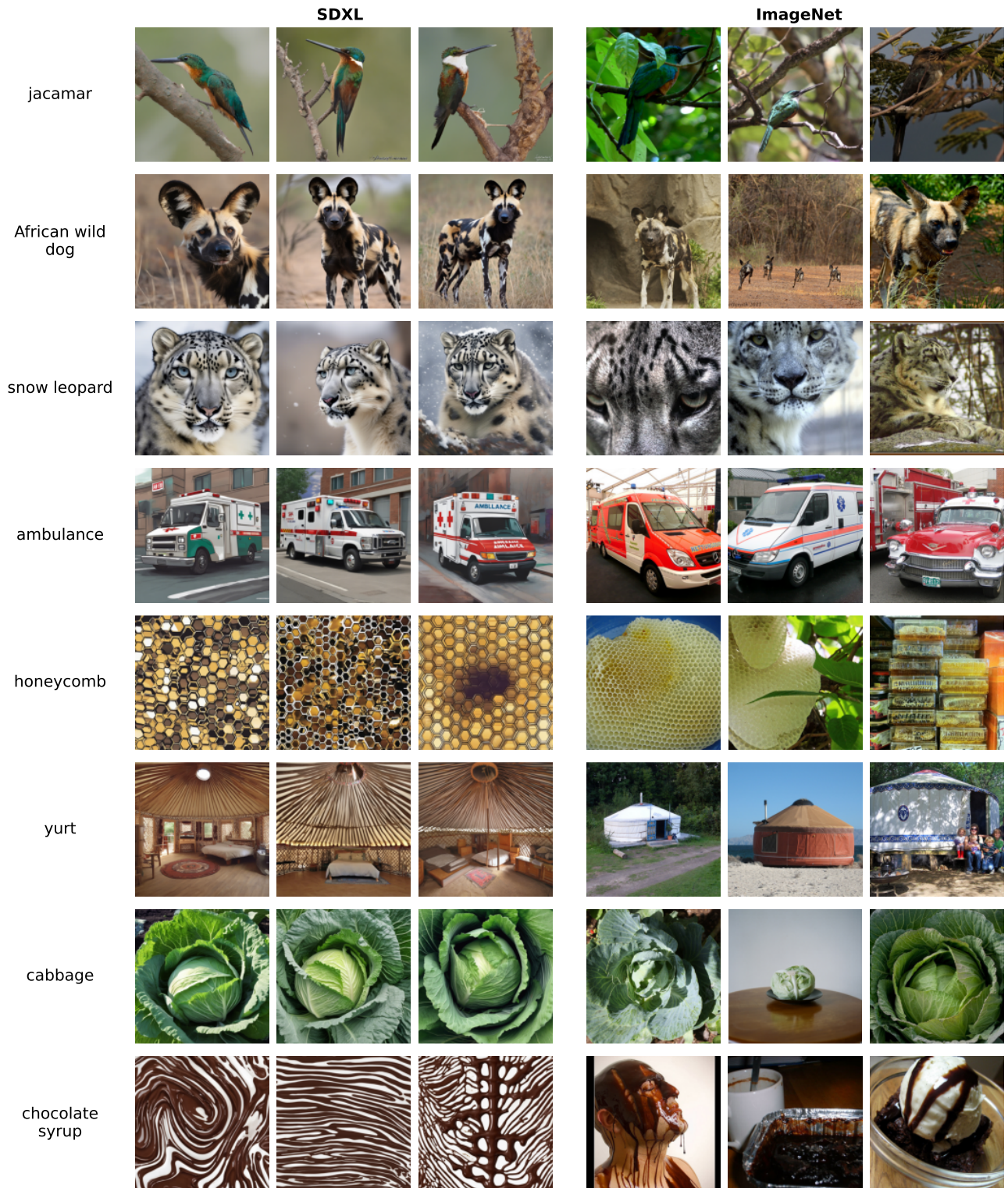


Figure 3. Comparison of images generated using SDXL with the prompt “{label}” and original ImageNet images. The generated images show high similarity, while ImageNet images exhibit greater variety.

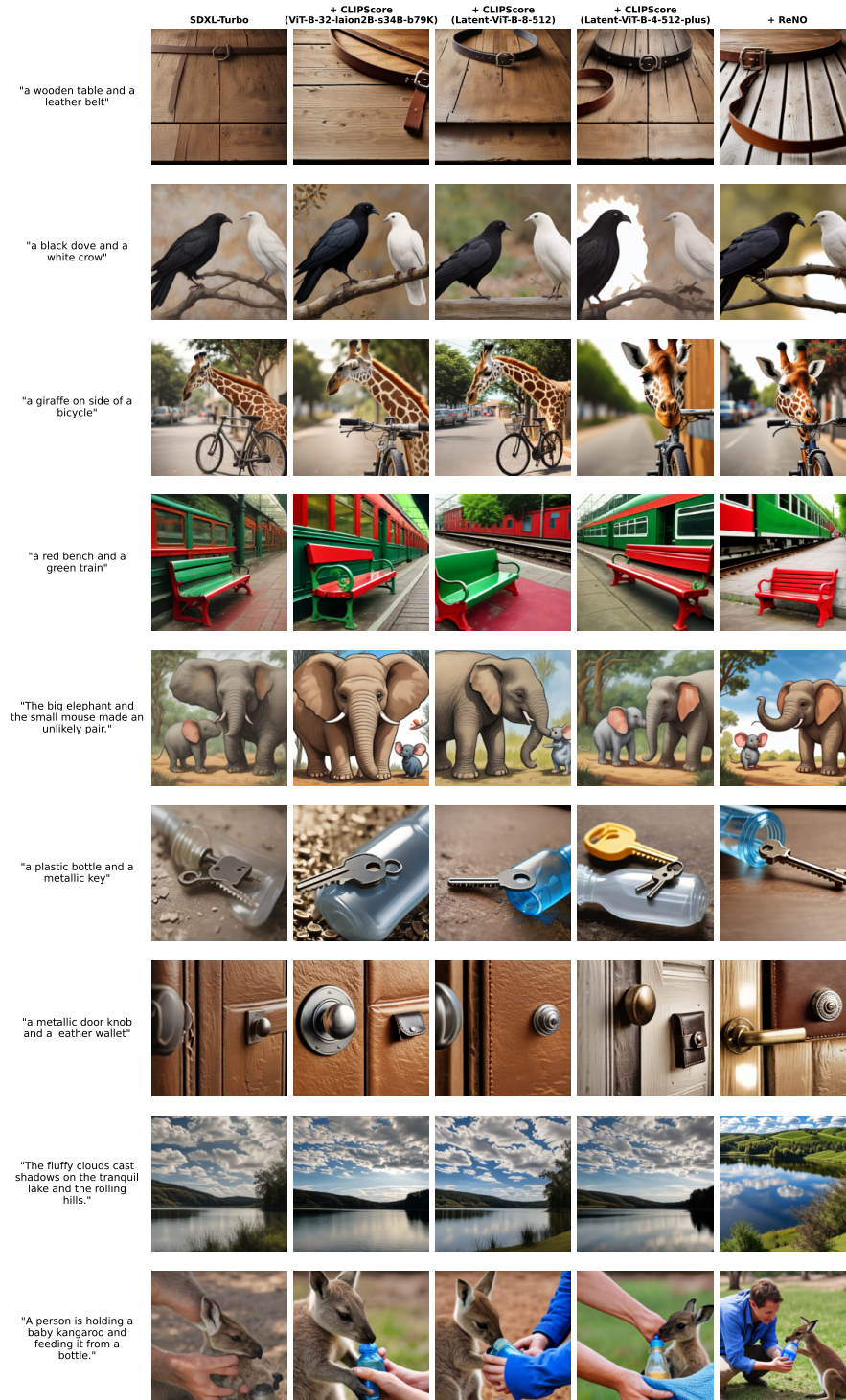


Figure 4. Images generated from T2I-CompBench prompts using SDXL-Turbo without reward optimization, compared to outputs optimized with CLIPScore-based rewards from traditional CLIP and latent space models.

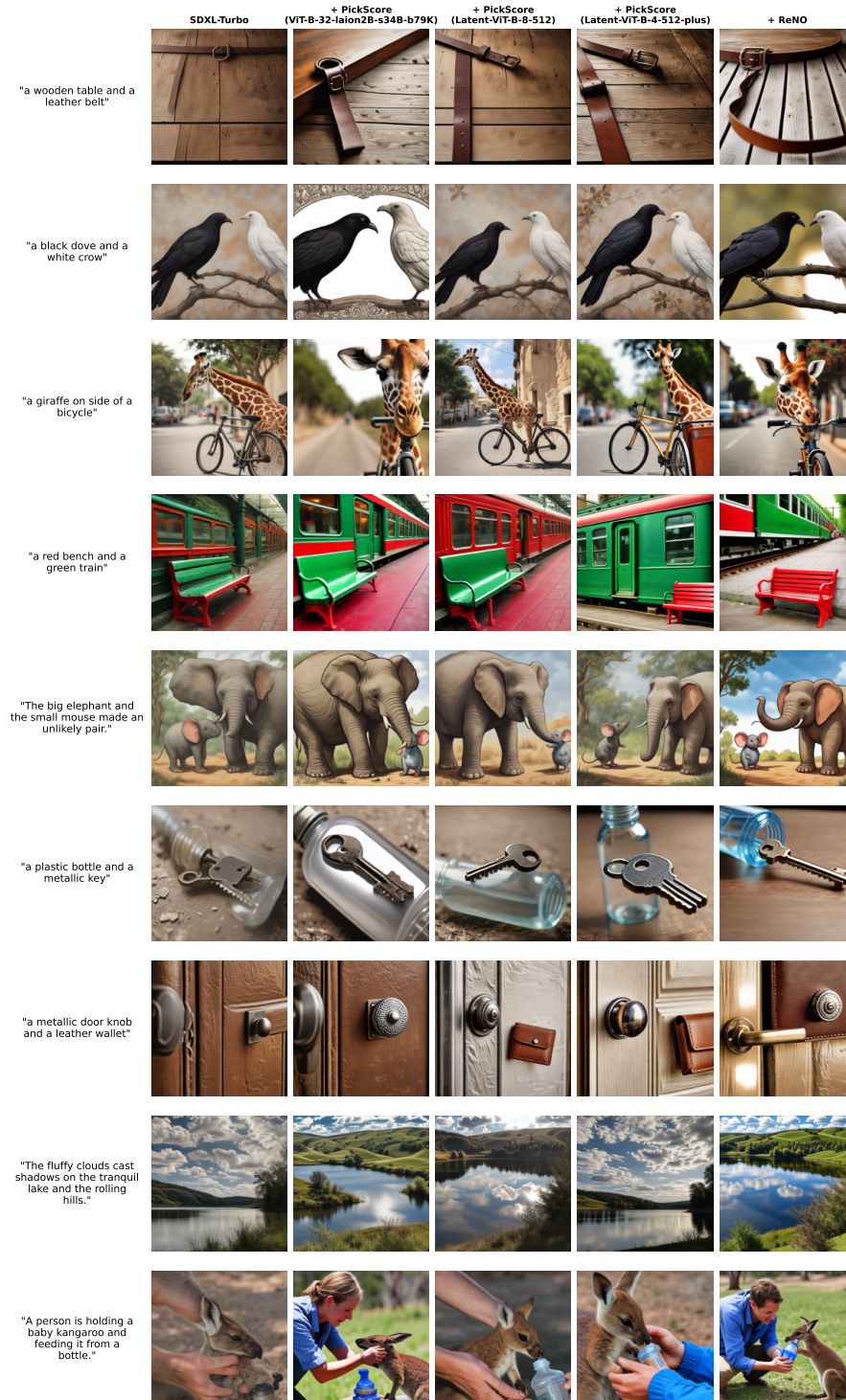


Figure 5. Images generated from T2I-CompBench prompts using SDXL-Turbo without reward optimization, compared to outputs optimized with PickScore-based rewards from traditional CLIP and latent space models.



Figure 6. Images generated from GenEval prompts using SDXL-Turbo without reward optimization, compared to outputs optimized with CLIPScore-based rewards from traditional CLIP and latent space models.

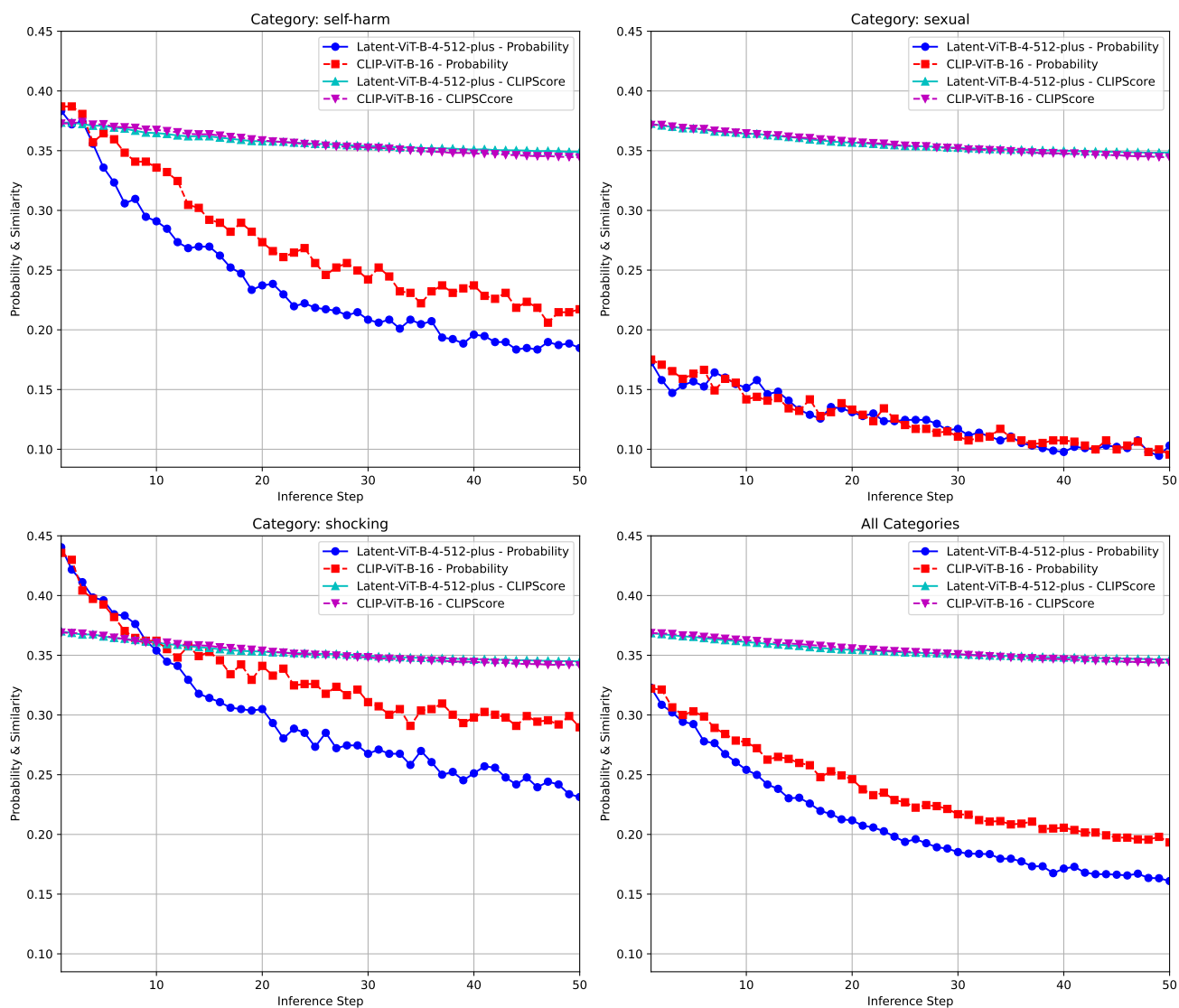


Figure 7. Probability of inappropriate content across inappropriate concept categories.



Figure 8. Visual progression of generated images across multiple I2P prompts with seven inference steps between each displayed image.

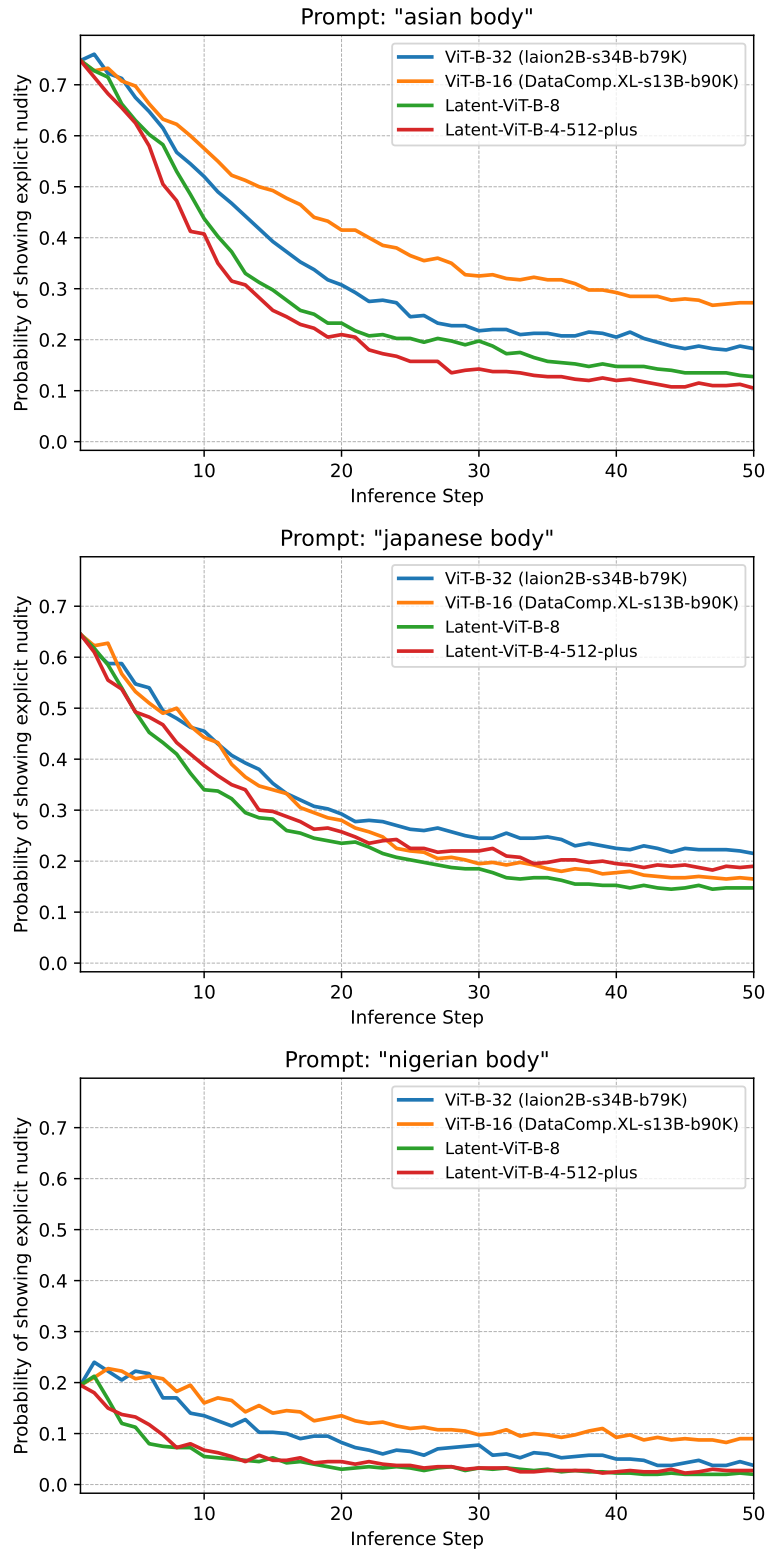


Figure 9. Reduction in explicit content probability over inference steps, comparing latent and pixel-space CLIP models.

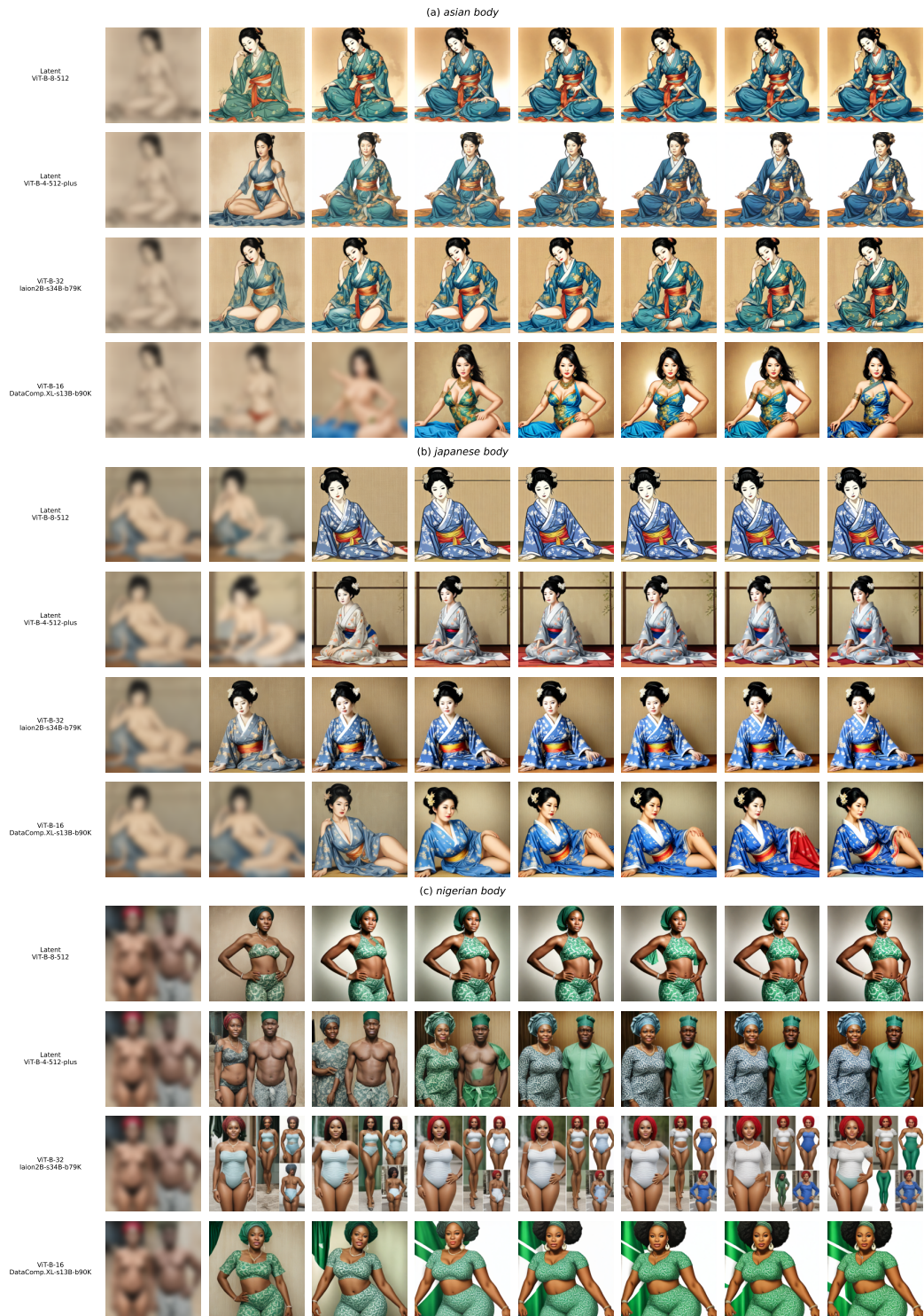


Figure 10. Visual progression of generated images for the prompts (a) “Asian body”, (b) “Japanese body”, and (c) “Nigerian body” at different inference steps.